Fracture and Fatigue-Crack Growth Behavior in Ductile-Phase Toughened Molybdenum Disilicide: Effects of Niobium Wire *vs* Particulate Reinforcements

K. BADRINARAYANAN, A.L. McKELVEY, K.T. VENKATESWARA RAO, and R.O. RITCHIE

A study has been made of the fracture toughness/resistance-curve (R-curve) and cyclic fatigue-crack propagation behavior in a molybdenum disilicide composite, ductile-phase toughened with nominally 20 vol pct Nb-wire mesh reinforcements ($Nb_m/MoSi_2$); results are compared with monolithic $MoSi_2$ and $MoSi_2$ reinforced with 20 vol pct spherical Nb particles ($Nb_p/MoSi_2$). It is found that the high aspect ratio wire reinforcements induce significant toughening in $MoSi_2$, both under monotonic and cyclic fatigue loading conditions. Specifically, the $Nb_m/MoSi_2$ composite exhibits R-curve behavior with a steady-state fracture toughness of ~13 MPa$\sqrt{m}$, compared to unstable fracture at K_c values below 5 MPa$\sqrt{m}$ in unreinforced $MoSi_2$ or $Nb_p/MoSi_2$. Such behavior is seen to be associated with extensive crack deflection within the reaction layer between Nb and the matrix, which leads to crack bridging by the unbroken ductile phase. Similarly, resistance to fatigue-crack growth is found to be far superior in the wire-reinforced composite over pure $MoSi_2$ and $Nb_p/MoSi_2$. Although crack paths are again characterized by extensive deflection along the Nb/matrix reaction layer, the role of crack bridging is diminished under cyclic loading due to fatigue failure of the Nb. Instead, the superior fatigue properties of the $Nb_m/MoSi_2$ composite are found to be associated with high levels of crack closure that result from highly deflected crack paths along the $(Nb,Mo)_5Si_3$ reaction layer interface.

I. INTRODUCTION

RECENTLY, there has been interest in silicide-based materials for high-temperature structural use for potential aerospace applications in the hot sections of future gas-turbine and high-performance engines.[1] Specifically, the intermetallic compound, $MoSi_2$ (body-centered tetragonal, $C11_b$ structure), has been considered to be an attractive candidate due to its high melting point (2020 °C) and excellent oxidation resistance at high temperatures. Furthermore, since it displays a brittle-to-ductile transition at around 1000 °C, it has better ductility than competitive ceramics for use at, and above, 1200 °C.[2–5]

However, like most other intermetallics at ambient temperatures, the fracture toughness of $MoSi_2$ is extremely low, *i.e.*, ~2 to 4 MPa$\sqrt{m}$; in fact, even at 1200 °C, its toughness is only 4.5 MPa$\sqrt{m}$.[1–11] Accordingly, the fracture toughness and damage tolerance of $MoSi_2$ must be significantly improved before this compound is seriously considered for use in structural applications.

Previous attempts to toughen $MoSi_2$ have invariably involved the addition of a second phase but have generally met with only limited success.[6–14] For example, the addition of brittle SiC fiber reinforcements was found to be detrimental due to matrix cracking arising from the high coefficient of thermal expansion mismatch between the reinforcement and matrix.[8] SiC whiskers, on the other hand, did increase the toughness by roughly a factor of 2,[6] as did CaO partially stabilized zirconia additions;[9] however, absolute toughness values were still well below 10 MPa$\sqrt{m}$. Corresponding fatigue and creep studies have also been performed on some of these materials.[10,11]

An alternative technique has been to use ductile reinforcements.[12–21] This approach is based on utilizing crack-tip shielding contributions arising primarily from tractions provided by the unbroken ductile ligaments bridging the crack wake to impede crack growth as the crack intercepts the ductile particles. Additional toughening can result from crack deflection[22] at the particle, crack blunting, and plastic deformation of the ductile phase, all of which critically depend on the nature of the interface; for example, partial debonding at the interface tends to relax constraint and increase the plastic energy dissipation. This toughening strategy has been successfully used in a variety of ceramic/metal and intermetallic/metal systems, including Al/glass,[15] Al/Al_2O_3,[16] Co/WC,[17] Nb/γ-TiAl,[18] TiNb/γ-TiAl,[19] Nb/Nb_5Si_3.[20] However, despite the effectiveness of such ductile-phase toughening for intermetallics under monotonic loading, limited studies on the cyclic fatigue behavior of these composites have shown that the mechanism is far less effective under cyclic loading conditions.[14,19]

In this context, the effects of ductile niobium reinforcements on the fracture and fatigue properties of $MoSi_2$ intermetallic alloy are examined in this study. Previous work[14] on $MoSi_2$ reinforced with (20 vol pct) spherical Nb particles ($Nb_p/MoSi_2$) indicated only a marginal increase in fracture toughness (*i.e.*, $K_c \approx 5.2$ MPa$\sqrt{m}$ for the composite

K. BADRINARAYANAN, formerly Graduate Student, Department of Materials Science and Mineral Engineering, University of California at Berkeley, is Photoetch Engineer with Cypress Semiconductors, San Jose, CA 95134. A.L. McKELVEY, Graduate Student, and R.O. RITCHIE, Professor, are with the Department of Materials Science and Mineral Engineering, University of California at Berkeley, Berkeley, CA 94720-1760. K.T. VENKATESWARA RAO, formerly Research Engineer, Department of Materials Science and Mineral Engineering, University of California at Berkeley, is Senior Engineer with Guidant Corp., Santa Clara, CA 95052.

Manuscript submitted November 14, 1995.

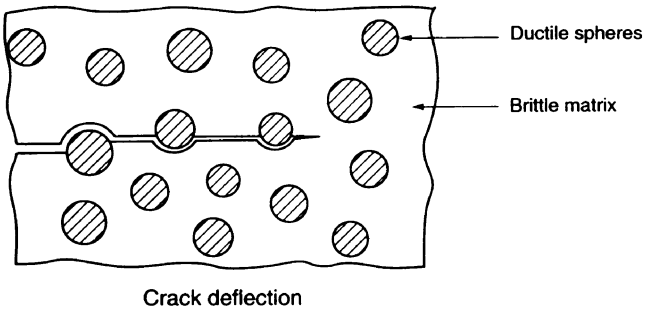

(*a*)

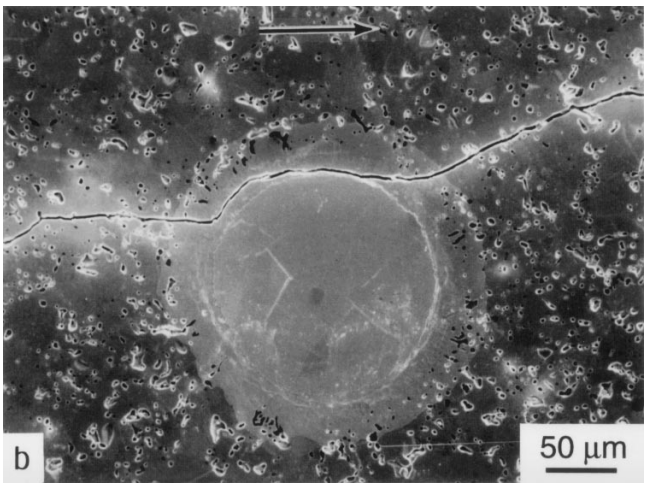

Fig. 1—(*a*) Schematic illustration and (*b*) SEM micrographs of crack-reinforcement interactions in $MoSi_2$ reinforced with Nb particulate ($Nb_p/MoSi_2$), showing stabilization of debonding around the Nb spheres within the weak $(Nb,Mo)_5Si_3$ reaction layer; this results in the crack circumventing the ductile phase with little or no crack bridging.[14] Arrow indicates direction of crack growth.

vs 4.2 MPa$\sqrt{m}$ for unreinforced $MoSi_2$); this was due to preferential debonding along the weak reaction layer between Nb and $MoSi_2$, which resulted in the crack simply circumventing the Nb spheres with little or no evidence of crack bridging (Figure 1). In view of these observations, it was reasoned that high aspect ratio reinforcements would promote ductile-phase bridging and substantially enhance crack path deflection. Accordingly, the objective of the present study is to investigate the influence of reinforcement geometry on ductile-phase toughening of $MoSi_2$, by examining the fracture and fatigue behavior in a nominally 20 vol pct chopped Nb-wire mesh reinforced $MoSi_2$ composite ($Nb_m/MoSi_2$) and comparing the results with those previously reported for the Nb-particulate reinforced material ($Nb_p/MoSi_2$).[14]

II. EXPERIMENTAL PROCEDURES

A. *Processing and Microstructure*

Prior work on $MoSi_2$ reinforced with Nb-wire mesh had shown excellent toughening potential for these brittle intermetallics.[23,24] Based on these earlier studies, Pickard and Ghosh (University of Michigan, Ann Arbor, MI) fabricated the Nb-wire mesh reinforced $MoSi_2$ composite used in the present research. The composite was fabricated by hot pressing a blended mixture of $MoSi_2$ powder and chopped Nb-wire mesh at ~1470 °C, the details of which have been provided in References 23 and 24. The resulting microstructure (Figure 2(a)) consisted of ~20 vol pct of (nominally) randomly distributed Nb wires, often in the form of a ''criss-crossed'' mesh. Following processing, the regular nature of the wire mesh was often distorted, with the individual wires having a diameter of $2r \sim 150$ to 200 μm and a length $h \sim 0.5$ to 1 mm. Consequently, the reinforcement had an aspect ratio (h/r) between ~7 to 13, compared to a value of unity for the spherical Nb-particulate reinforcements.

The $Nb_p/MoSi_2$ composites were fabricated by hot isostatically pressing −325 mesh $MoSi_2$ and −35 to +80 mesh spherical Nb particles at 1700 °C for 1 hour under 200 MPa pressure; details are reported in Reference 14.

A reaction interface can be seen between the Nb and $MoSi_2$ in both Nb_p and Nb_m composites (Figure 2(b)). The interface thickness is ~40 μm, with a composition indicative of Nb_5Si_3 stoichiometry close to the Nb and Mo_5Si_3 close to the matrix. The relative atomic percentages of Mo, Si, and Nb, evaluated using energy dispersive spectroscopy, are indicated in Table I. This reaction layer is known to have low toughness.[25,26] Corresponding physical and mechanical properties of the $MoSi_2$ and Nb are listed in Table II.

B. *R-Curve Measurements*

The fracture toughness behavior of the Nb-wire reinforced composite was evaluated under plane strain conditions* by monotonically loading fatigue precracked, disk-shaped compact DC(T) specimens (of diameter 25 mm, width $W = 19$ mm, and thickness $B = 2.5$ mm) to failure; a minimum of two samples were evaluated per test condition. Resistance-curve (R-curve) behavior was then determined in terms of the crack-growth resistance, K_R, as a function of the crack extension, Δa. Crack lengths were measured using unloading elastic compliance derived from a 350 ohm strain gage attached to the backface of the specimen;[28] estimates were verified by comparison to crack length values measured optically with a Questar telescope (with 5-μm resolution). Typically, the compliance estimates of crack length were found to be approximately 5 pct less than the optical values, typically, by ~0.03 W, consistent with the presence of crack bridging under monotonic loading.[29] Consequently, compliance-based estimates of crack length were corrected to account for the change in compliance associated with such bridging.

Fracture surfaces were imaged in the scanning electron microscope (SEM). In addition, crack profiles were obtained by metallographic sectioning and polishing of the tested sample; surfaces were coated with a thin gold-palladium coating prior to examination in the SEM.

C. *Cyclic Fatigue Testing*

Cyclic fatigue-crack growth behavior in the Nb-wire reinforced composite was examined under tension-tension

*Previous studies[27] have shown that no plasticity is evident below 950 °C in $MoSi_2$ with similar microstructure. Even with the assumption of a lower-bound composite yield strength of 300 MPa, the maximum plastic zone sizes at a K of 13 MPa$\sqrt{m}$ would be of the order of 250 μm, which is small compared to the specimen thickness.

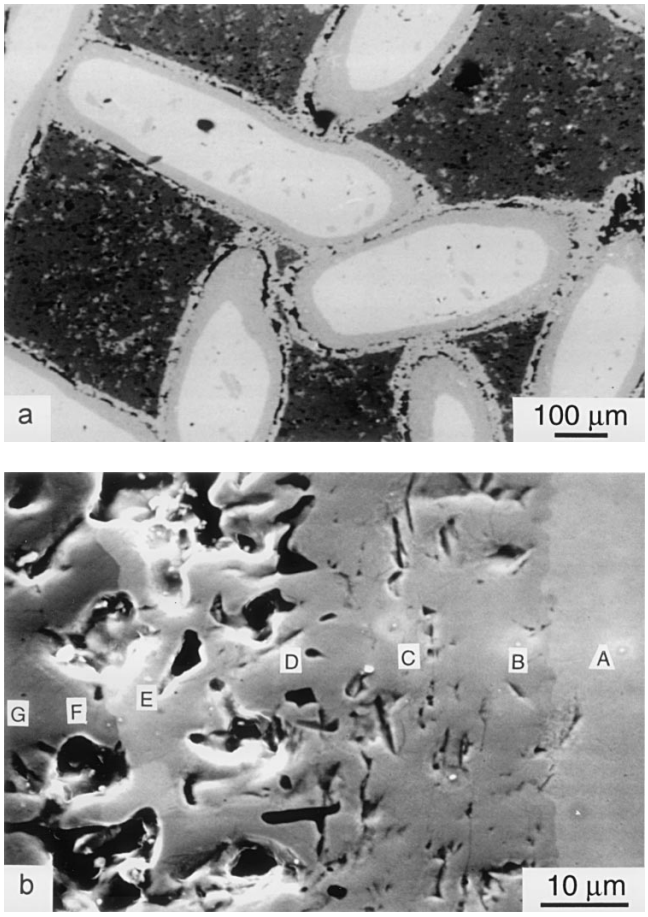

Fig. 2—Scanning electron micrographs of the microstructure of the $Nb_m/MoSi_2$ composite, showing (*a*) a representative distribution of the 20 vol pct Nb-wire mesh reinforcement (light regions) within the $MoSi_2$ matrix (dark regions) and (*b*) ~40-μm-thick, Nb mesh/$MoSi_2$ reaction interface. Energy-dispersive spectroscopy analyses of the regions marked from A through G are given in Table I.

Table I. Composition in Atomic Percent of the Reaction Layer between the $MoSi_2$ and Nb in Figure 2(b), as Determined Using Energy-Dispersive Spectroscopy

Region	Mo	Si	Nb	Phase
A	0.0	1.3	98.7	pure Nb
B	1.1	36.3	62.7	$\sim Nb_5Si_3$
C	2.1	37.3	60.7	$\sim Nb_5Si_3$
D	22.8	37.6	39.6	$\sim (Nb,Mo)_5Si_3$
E	52.0	39.3	8.8	$\sim (Mo,Nb)_5Si_3$
F	34.4	63.7	1.9	$\sim MoSi_2$
G	34.5	65.5	0.0	$\sim MoSi_2$

loading using identical disk-shaped compact specimens, with a wedge-shaped starter notch to assist precracking. Testing was performed in ambient air (22 °C, 45 pct relative humidity) on automated servohydraulic testing machines operating under load or stress-intensity control at load ratios ($R = K_{min}/K_{max}$) between 0.1 and 0.7 at a frequency of 25 Hz (sine wave). Procedures essentially conform to ASTM Standard E647,[30] modified for brittle materials.[31] Growth rates were obtained over the range $\sim 10^{-11}$ to 10^{-7} m/cycle under both *K*-decreasing and *K*-increasing conditions (with a normalized *K* gradient of ± 0.10 mm^{-1}).* Crack lengths were continuously monitored *in situ* using backface strain based unloading elastic-compliance measurements,[28] and were verified periodically by optical microscopy. For fatigue-crack growth, good agreement to within 2 pct was found between optical and compliance measurements of crack length, consistent with a diminished effect of bridging under cyclic loads;[29] this is in contrast to differences of ~5 pct seen under monotonic loading. Data are presented in terms of the growth rate per cycle (*da*/*dN*), as a function of applied stress-intensity range, given by the difference in the maximum and minimum stress intensities during the cycle ($\Delta K = K_{max} - K_{min}$). Similar to the R-curve tests, fatigue fracture surfaces and crack profiles were examined in the SEM.

Table II. Physical and Mechanical Properties of $MoSi_2$ and Nb[1–13]

Property	$MoSi_2$	Nb
Density (g/cm^3)	6.24	8.57
Crystal structure	bct	bcc
Melting point (°C)	2020	2468
Coefficient of thermal expansion, α		
at 20 °C	$\sim 6.8 \times 10^{-6}$	$\sim 7.3 \times 10^{-6}$
at 1200 °C	$\sim 10 \times 10^{-6}$	$\sim 9.6 \times 10^{-6}$
Young's modulus, *E* (GPa)	440	103
Poisson's ratio, *v*	0.17	0.38
Tensile strength at 20 °C (MPa)	325	170
Yield strength at 1200 °C (MPa)	325	55
Brittle-ductile transition temperature (°C)	~1000 to 1200	−100

*This load-shedding rate is deemed to be conservative with respect to the measurement of the fatigue threshold in most ductile materials.[30] We expect a minimal effect of the load-shedding rate in the present intermetallic composite, due to the limited plasticity.

In addition, an assessment of the extent of crack closure was made from traces of load *vs* backface strain measurements; such closure is defined in the metals literature as premature contact of the crack surfaces occurring at loads above the minimum load during the fatigue cycle.[32,33] Conventionally, the closure stress intensity, K_{cl}, associated with the closure load can be estimated at the point of deviation from linearity of the elastic compliance on the unloading part of the cycle.[32,33] This was achieved by monitoring changes in the correlation coefficient of a linear regression fit to the load *vs* displacement data, as described in Reference 34. Using such measurements, an effective (near-tip) stress-intensity range is usually defined as $\Delta K_{eff} = K_{max} - K_{cl}$ (for $K_{cl} \geq K_{min}$),[32] although its interpretation is somewhat questionable in materials undergoing crack bridging where there is already contact between the crack faces.

III. RESULTS

A. *R-Curve Behavior*

The measured R-curve behavior is shown in Figure 3 and clearly indicates that the addition of the Nb-wire mesh reinforcement provides for significant toughening in $MoSi_2$. Compared to the toughness of unreinforced $MoSi_2$, which

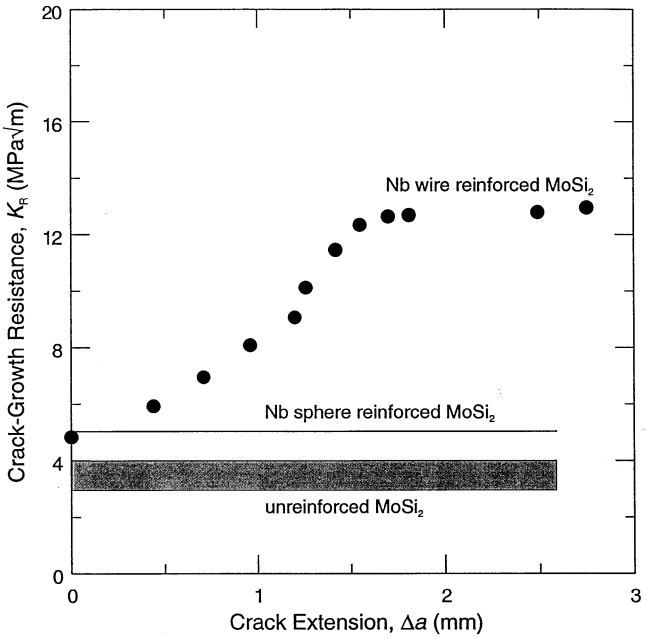

Fig. 3—Resistance curves for Nb-wire reinforced $MoSi_2$, compared to that for Nb-particulate $MoSi_2$[14] and the unreinforced matrix material. Note that the R curve for the $Nb_m/MoSi_2$ composite shows a plateau after $\Delta a \sim 1.5$ mm, which is estimated to be the length, l_{ssb}, of the bridging zone.

showed no R curve and failed catastrophically at a K_c value of ~4 MPa$\sqrt{m}$, the composite shows a slight elevation in crack-initiation toughness to 4.8 MPa$\sqrt{m}$; subsequently, the crack advances at higher applied stress intensities reaching a steady-state (''plateau'') toughness of 13 MPa$\sqrt{m}$ after ~1.5 mm of crack extension. Such a threefold increase in toughness is to be compared with that of spherical Nb_p-reinforced $MoSi_2$, where, similar to the unreinforced matrix, no R-curve behavior was seen and unstable fracture occurred at K_c of ~5.2 MPa$\sqrt{m}$.[22]

The enhanced toughness of the $Nb_m/MoSi_2$ composite can be related to the interaction of the crack with the short Nb fibers. The SEM observations, shown in Figure 4, reveal pronounced crack deflection associated with debonding within the reaction layer and crack advance along the Nb/reaction-layer interface. Figure 4(a) shows an example where the crack has renucleated across a Nb wire roughly 600 μm behind the crack tip (marked A-A); this results in the creation of an intact Nb ligament which acts as a bridge across the crack faces. At further distances behind the tip, the Nb ligaments are cracked (Figure 4(b)), consistent with the observed plateau in the R curve (which is indicative of a steady-state shielding zone) for crack extensions larger than ~1.5 mm. As noted previously, such crack bridging can be detected in terms of the differing estimates of crack length based on elastic compliance (representing the bridged crack) and optical measurements (representing the unbridged crack).[29] In the present case, the compliance-based (bridged) effective crack length was ~2.15 mm when the R curve reached a plateau toughness of ~13 MPa$\sqrt{m}$; this occurred after roughly 2.75 mm of crack extension (measured optically), indicating that the bridging zone was larger than ~600 μm. Indeed, the R-curve data in Figure 3 suggest that this steady-state bridging zone exists for approximately 1.5 mm behind the crack tip.

In comparison, no appreciable toughening was apparent

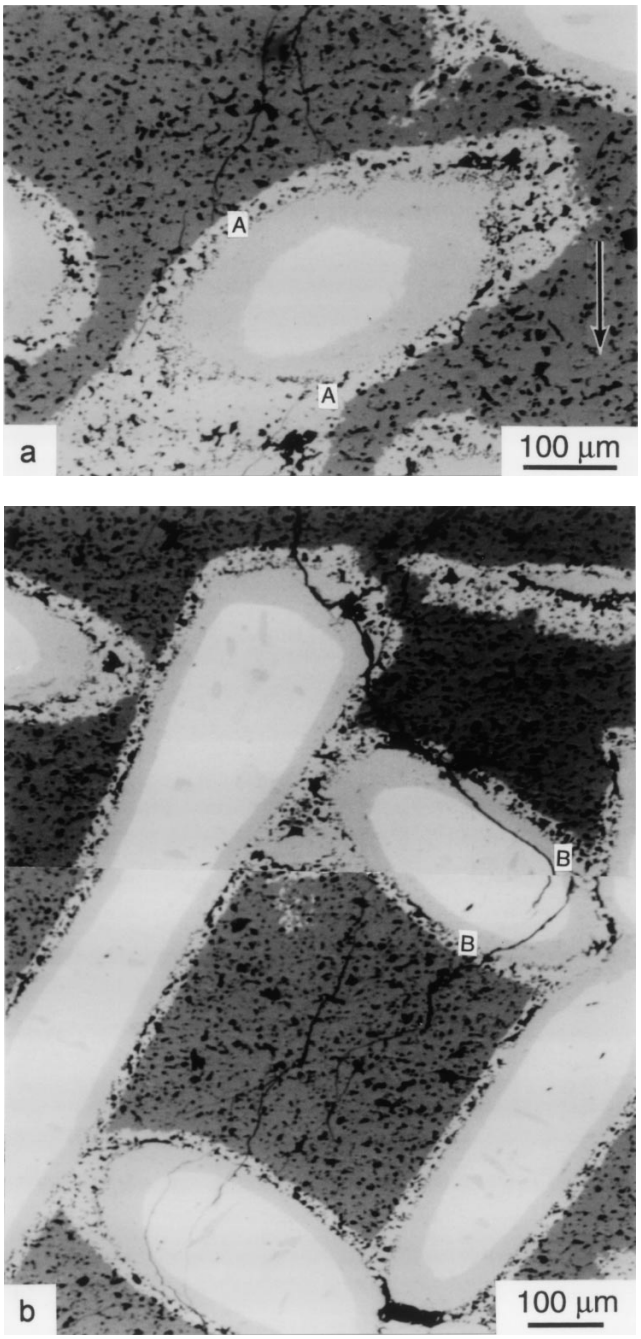

Fig. 4—Crack–Nb-wire reinforcement interactions in the $Nb_m/MoSi_2$ composite under monotonic loading, showing (*a*) crack bridging by an intact Nb wire (marked A-A) situated at ~600 μm, behind the crack tip, and (*b*) pronounced crack deflection along the weak reaction-layer interface and fracture (marked B-B) of a Nb-wire ligament situated beyond the bridging zone, *i.e.*, at ~1.6 mm behind the tip. The arrow indicates the general direction of crack growth.

in the Nb-sphere reinforced $MoSi_2$, primarily due to the lack of crack bridging by the Nb phase. The crack merely circumvented the Nb particles by debonding along the weak $(Nb,Mo)_5Si_3$ reaction-layer interface (Figure 1), leading to a minimal increase in toughness from 4.2 MPa$\sqrt{m}$ (in unreinforced $MoSi_2$) to 5.2 MPa$\sqrt{m}$ (in the composite), arising principally from crack deflection in the reaction layer and resultant crack-path tortuosity.[14]

Corresponding fracture surfaces are shown in Figure 5.

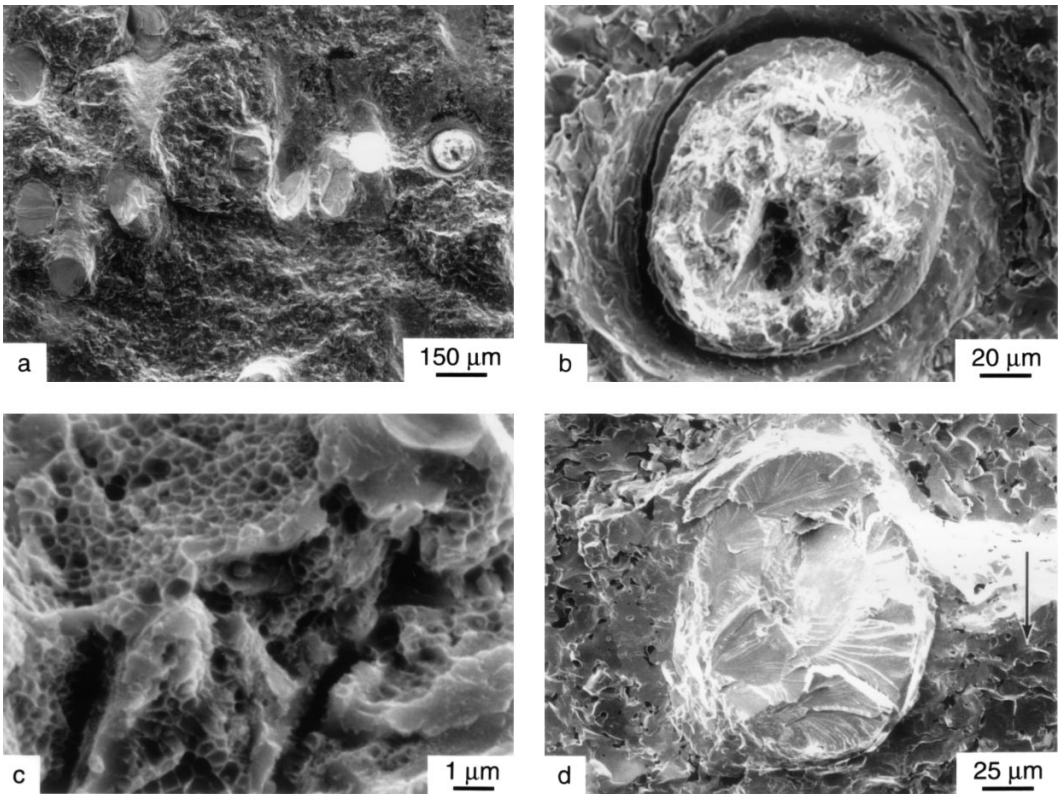

Fig. 5—Scanning electron micrographs of the fracture surfaces in the $Nb_m/MoSi_2$ composite under monotonic loading, showing (*a*) fracture morphology at low magnification, (*b*) and (*c*) failure of a Nb wire by ductile tearing with some transgranular cleavage (where the Nb wire has debonded from the matrix), and (*d*) failure of another Nb wire by transgranular cleavage (where no such debonding has occurred). The arrow indicates the general direction of crack growth.

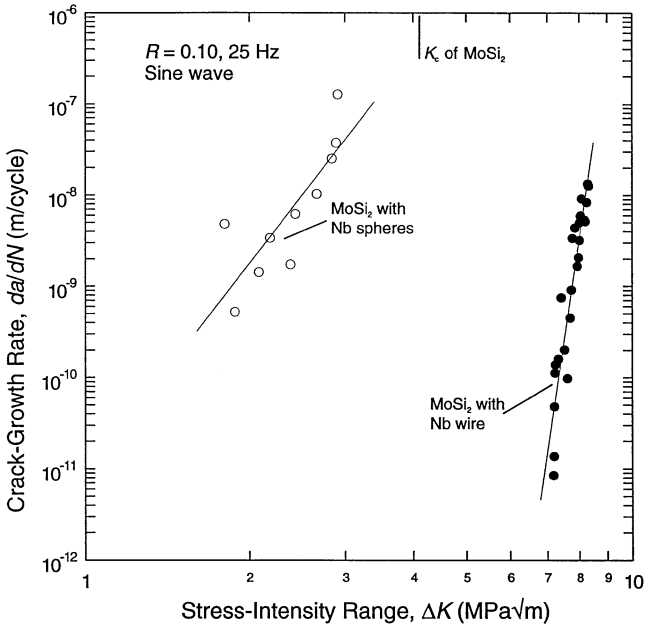

Fig. 6—Variation in cyclic fatigue-crack growth rates, da/dN, as a function of the nominal (applied) stress-intensity range, ΔK ($=K_{max} - K_{min}$), at $R = 0.1$ for $MoSi_2$ reinforced with 20 vol pct Nb in the form of high-aspect ratio wire mesh ($Nb_m/MoSi_2$) and as spherical particulates ($Nb_p/MoSi_2$).

Similar to behavior reported for Nb/Nb_5Si_3 composites,[20,35,36] the failure of the Nb occurs by both ductile and brittle modes (Figure 5(a)), *i.e.*, ductile tearing (Figures 5(b) and (c)) and transgranular cleavage (Figure 5(d)), presumably dependent upon the effective size of the reinforcement and the degree of constraint associated with the extent of interface debonding. For example, Figure 5(b) shows a Nb wire oriented along the loading axis that failed primarily by ductile microvoid coalescence (Figure 5(c)) with isolated regions of cleavage fracture; in this case, the partial debonding between the Nb wire and the matrix assists in reducing constraint and promoting the ductile failure. Conversely, where such interfacial cracking did not take place, the Nb failed by transgranular cleavage (Figure 5(d)). Corresponding fracture in the $MoSi_2$ matrix was transgranular (Figure 5(a)).

B. *Fatigue-Crack Propagation Behavior*

The cyclic fatigue results are shown in Figure 6 for $R = 0.1$; here, the variation in crack-growth rates is plotted as a function of applied ΔK for the Nb-wire reinforced $MoSi_2$ and compared with previous results[14] on the Nb-particulate reinforced material. Data for the $Nb_m/MoSi_2$ composite were obtained between $\sim 10^{-11}$ to 10^{-7} m/cycle over a narrow range of stress intensities (*i.e.*, 7.2 to 8.3 $MPa\sqrt{m}$), indicating that, similar to most low-ductility ceramics and intermetallics, growth rates are strongly dependent upon ΔK. In terms of a Paris power-law type formulation,[37] results can be simply expressed in terms of scaling constants C and m as

$$da/dN = C\Delta K^m \qquad [1]$$

For $Nb_m/MoSi_2$, the exponent m is extremely high (m values

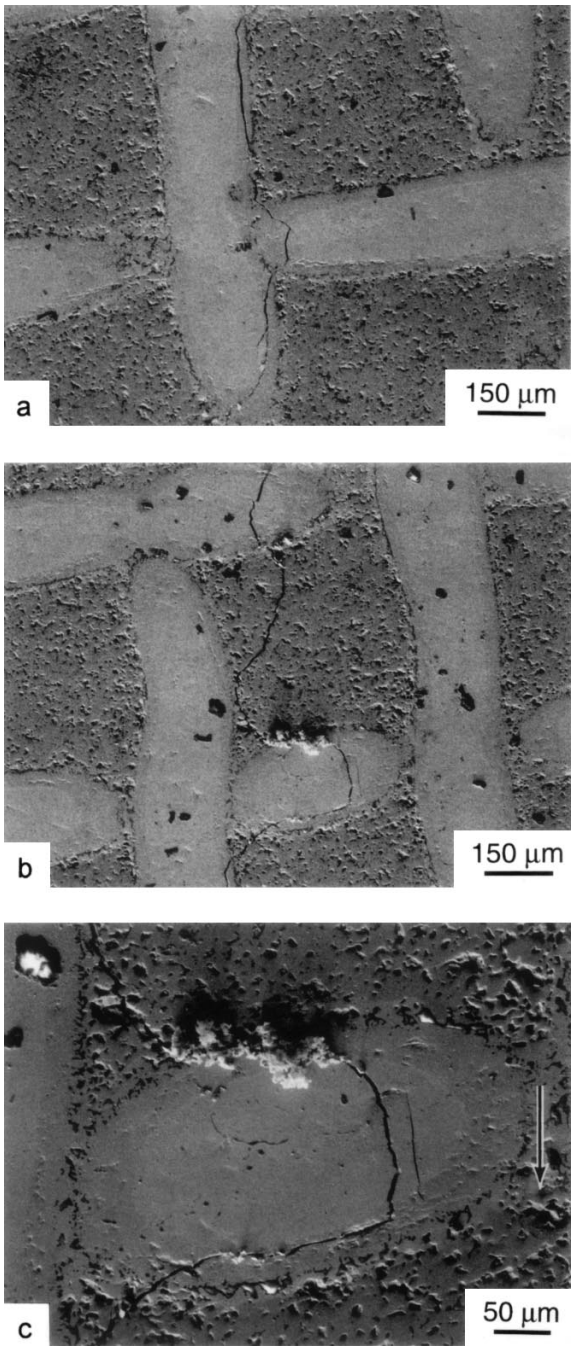

Fig. 7—Scanning electron micrographs of the crack/Nb wire interactions under cyclic fatigue loading in the $Nb_m/MoSi_2$ composite, showing (*a*) cracking along the weak reaction-layer interface and (*b*) and (*c*) failure of the Nb phase (which limits any ductile-phase bridging). Note the failure of the Nb ligament in (c) away from the primary crack plane and the presence of debris as a result of repetitive crack sliding at the interface. The arrow indicates the direction of crack growth.

for results at the different load ratios exceed ~20, as discussed subsequently); a corresponding value for $Nb_p/MoSi_2$ was found to be $m = 14$. It is apparent that despite a higher sensitivity to stress intensity, crack-growth rates in the present wire-reinforced composite are orders of magnitude slower than in the particulate-reinforced material. Indeed, the fatigue-crack growth threshold, ΔK_{TH}, estimated at a minimum growth rate of 10^{-11} m/cycle, is ~7.2 MPa$\sqrt{m}$ in $Nb_m/MoSi_2$, compared to roughly 2 MPa$\sqrt{m}$ in $Nb_p/MoSi_2$;[14] these values are nominally 0.4 to 0.6 of the (maximum) K_c values.

Similar to that seen under monotonic loading (Figure 4(b)), the crack path in fatigue involves extensive crack deflection along the $(Nb,Mo)_5Si_3$ reaction-layer interface (Figure 7). However, in contrast to behavior under monotonic loading, little evidence of crack bridging by intact Nb-wire ligaments could be detected; in fact, all the Nb regions that intersected the crack path were observed to be broken (Figure 7). Such observations were confirmed experimentally in that crack length measurements based on elastic compliance and visual examination were essentially identical.[29]

In several cases, however, the intersected Nb wire failed several hundred microns above the main plane of the fatigue crack (Figure 7(c)) after interfacial cracking at deflection angles of almost 90 deg. In these instances, the presence of debris can also be observed at the crack mouth, suggesting some contribution to crack-tip shielding from debonding and repetitive frictional sliding between the Nb and the reaction-layer/matrix (akin to fiber or grain pullout in fiber composites or grain-bridging ceramics[38]).

The degradation in crack bridging in cyclic fatigue due to the premature failure of the ductile phase has been reported for several other ductile-phase toughened intermetallic systems, including TiNb/γ-TiAl,[14] Nb/γ-TiAl,[39] and Nb/Nb_3Al.[40] Indeed, in many comparable ceramic systems, it is the cycle-dependent decay in crack-tip shielding that is the primary mechanism inducing fatigue crack advance.[38] However, despite the diminished role of ductile-particle bridging, the fatigue-crack growth properties of the Nb-mesh reinforced $MoSi_2$ composite are far superior to spherical $Nb_p/MoSi_2$ composites and unreinforced $MoSi_2$. Stable fatigue-crack growth could not be detected in pure $MoSi_2$; samples failed catastrophically at ΔK levels of ~4 MPa$\sqrt{m}$ ($R = 0.1$) after less than 50 μm of apparent crack growth, detected from changes in specimen compliance.

Fractographically, cyclic fatigue surfaces in the $Nb_m/MoSi_2$ composite show significant roughness (Figure 8) arising from the crack-path tortuosity associated with deflection at the many reaction-layer interfaces of the Nb fibers (Figure 7). Such roughness is consistent with the very high observed levels of crack closure, which, at ΔK levels less than ~7.5 MPa$\sqrt{m}$, ($R = 0.1$) are associated with K_{cl} values as high as 50 pct of K_{max} (Figure 9). Although fatigue failure in the $MoSi_2$ matrix resembles the transgranular cleavage seen under monotonic loading (Figure 8(a)), the Nb conversely appears to fail by transgranular cleavage (Figure 8(b)) and quasi-cleavage mechanisms (Figure 8(c)). Similar to observations along the crack flanks, evidence of wear debris is also apparent on the fatigue fracture surfaces, particularly around the grain corners. It is presumed that such debris is the result of repetitive sliding between the crack faces and asperity damage during unloading, near Nb wires which have fractured away from the primary crack plane or have pulled out (Figure 8(a)).

C. *Influence of Load Ratio*

Additional cyclic fatigue-crack propagation tests were conducted on the $Nb_m/MoSi_2$ composite at load ratios of 0.3, 0.5, and 0.7; crack-growth rate results are plotted as a function of the applied ΔK in Figure 10. Similar to most

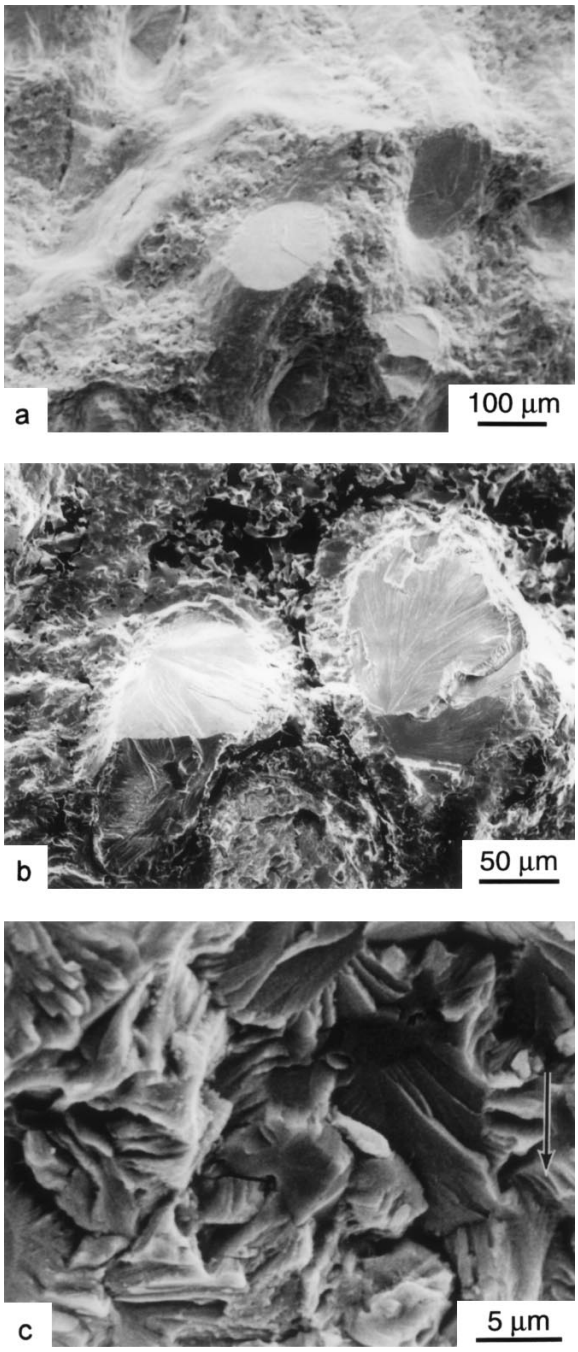

Fig. 8—(*a*) Scanning electron micrographs of the fatigue fracture surfaces in the $Nb_m/MoSi_2$ composite at $R = 0.1$, showing (*a*) morphology at low magnification and failure of a Nb wire (*b*) by transgranular cleavage and (*c*) by a quasi-cleavage mode. Note evidence of wear at the grain corners and debris on the fatigue surfaces. The arrow indicates the general direction of crack growth.

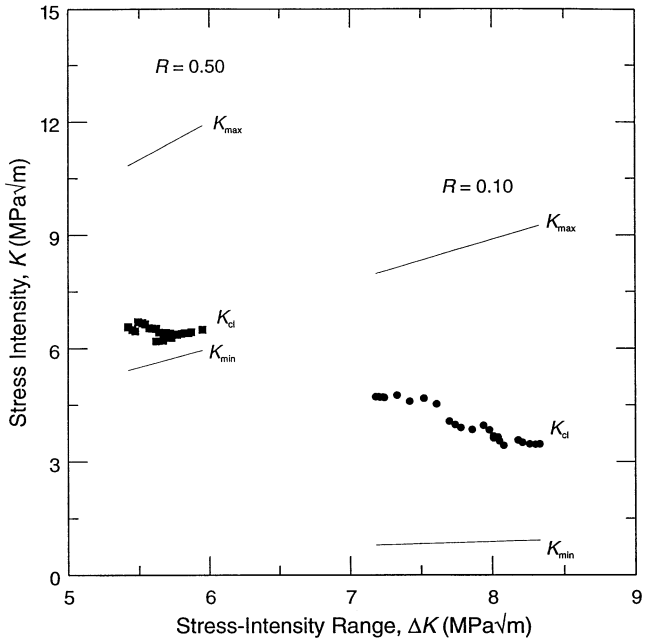

Fig. 9—Variation in measured crack closure in the $Nb_m/MoSi_2$ composite, plotted as the maximum, minimum, and closure stress intensities, K_{max}, K_{min}, and K_{cl} respectively, as a function of nominal stress-intensity range, ΔK, at load ratios of $R = 0.1$ and 0.5.

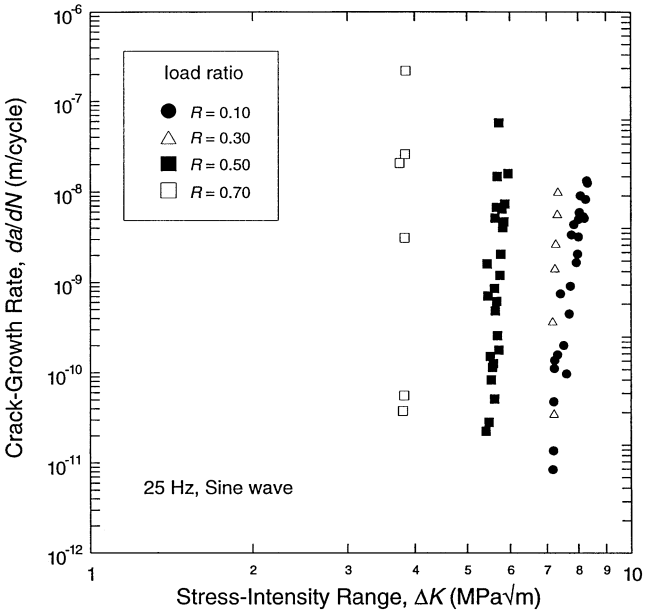

Fig. 10—Variation in cyclic fatigue-crack growth rates, da/dN, for a range of load ratios from $R = 0.1$ to 0.7, in the $Nb_m/MoSi_2$ composite as a function of the applied stress-intensity range, $\Delta K = K_{max} - K_{min}$.

metals and ceramics, increasing the load ratio or mean stress of the loading cycle is found to increase the rates of fatigue-crack propagation and reduce the fatigue thresholds (Table III). However, unlike metals, growth rates show a much higher dependency on K_{max}. This is apparent by simply expressing the data in terms of a modified Paris power-law relationship which includes the effect of both ΔK and K_{max},[41] *viz*.

$$da/dN = C' (K_{max})^n (\Delta K)^p \qquad [2]$$

where C' is a scaling constant (independent of K_{max}, ΔK, and R) and n and p are experimentally determined crack-growth exponents. Equation [2] can be related to Eq. [1] by noting that $K_{max} = \Delta K/(1\text{-}R)$, such that nominally $m = n + p$ and $C = C'/(1\text{-}R)^n$. A regression fit to the data for $Nb_m/MoSi_2$ in Figure 10 yields

$$da/dN = 6.31 \times 10^{-29} (K_{max})^{13.2} (\Delta K)^{7.5} \qquad [3]$$

(units: m/cycle, MPa$\sqrt{\text{m}}$), which clearly illustrates the higher sensitivity of the growth rates to K_{max}. This is in

Table III. Summary of Fatigue Threshold Data in $Nb/MoSi_2$ Composites

Material	Load Ratio (R)	Fatigue Threshold, ΔK_{TH} (MPa$\sqrt{m}$)
$Nb_m/MoSi_2$	0.1	7.2
—	0.3	7.2
—	0.5	5.4
—	0.7	3.8
$Nb_p/MoSi_2$	0.1	<1.8

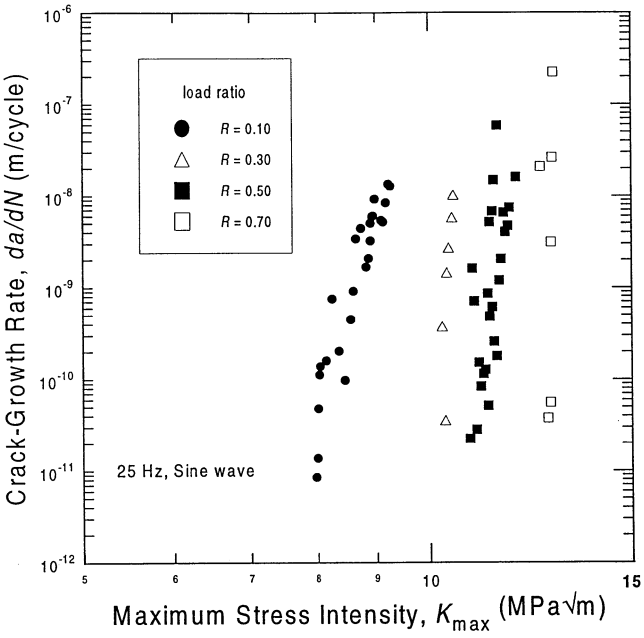

Fig. 11—Variation in cyclic fatigue-crack growth rates, da/dN, for a range of load ratios from $R = 0.1$ to 0.7, in the $Nb_m/MoSi_2$ composite as a function of the maximum stress intensity, K_{max}.

contrast to metals where $p > n$ (typical values for a Ni-base superalloy are $p \sim 3$ and $n \sim 0.4$)[42] and in ceramics where $p << n$ (typical values for Si_3N_4 are $p \sim 1.3$ and $n \sim 29$).[43] Because of this extreme dependency on K_{max}, plotting crack-growth data in most nontransforming monolithic ceramics in terms of K_{max} provides an effective normalization of the role of load ratio on fatigue-crack growth;[38,41,43] however, no such characterization is apparent for the present $MoSi_2$ composites (Figure 11). The fact that the dependency of load ratio can be effectively normalized by plotting in terms of K_{max} in ceramics results from the correspondingly small dependency of growth rates on ΔK. This follows because the crack-advance mechanism in these materials is essentially identical to that occurring under monotonic (*i.e.*, static fatigue) loading; the small ΔK dependence simply results from a cycle-dependent degradation in crack-tip shielding (*e.g.*, by crack bridging) in the crack wake.[38,43] Similarly, there appears to be no intrinsic mechanism of cyclic fatigue-crack advance in the $MoSi_2$ matrix; it fails simply by transgranular cleavage as under monotonic and cyclic loads. Crack growth in the ductile phase and along the matrix/Nb reaction layer in the $Nb_m/MoSi_2$ composite, conversely, is a cyclically motivated process (failure modes are different for monotonic and cyclic loading, Figures 5 and 8); the resulting increased ΔK dependency thus precludes a normalization of growth rates in terms of K_{max}.

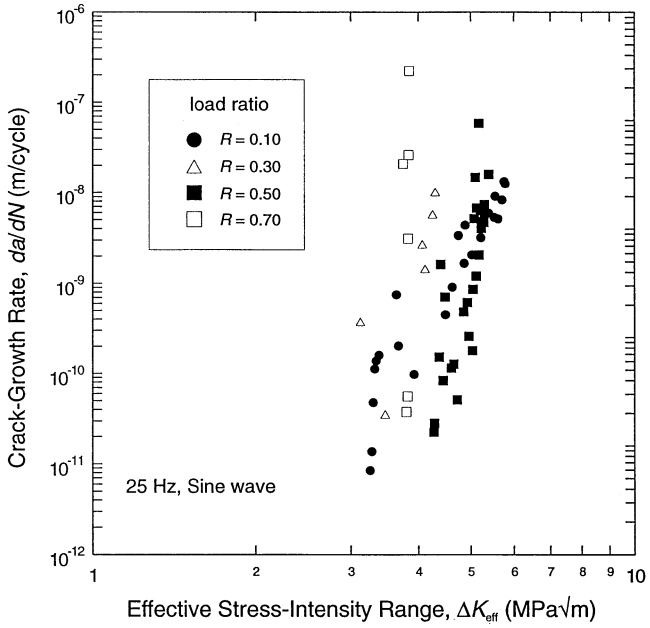

Fig. 12—Variation in cyclic fatigue-crack growth rates, da/dN, for a range of load ratios from $R = 0.1$ to 0.7, in the $Nb_m/MoSi_2$ composite as a function of the effective stress-intensity range, ΔK_{eff} ($=K_{max} - K_{cl}$), to allow for the influence of crack closure.

Corresponding crack closure (K_{cl}) levels measured at $R = 0.1$ and 0.5 are shown in Figure 9; no appreciable closure was detected at $R = 0.7$. Although there is some uncertainty in the interpretation of such results, they do indicate that the low-R data are most affected by crack closure. Indeed, the closure stress intensity increases with a decrease in ΔK, which is characteristic in metals of a roughness-induced crack closure mechanism[33,44] associated with the wedging and sliding action between mating fracture-surface asperities (Figure 7(c)). Accordingly, growth rates in the $Nb_m/MoSi_2$ composite can be replotted in terms of an effective (near-tip) driving force, ΔK_{eff} ($= K_{max}$-K_{cl}) to allow for such closure. As shown in Figure 12, this approach provides a better correlation for the dependency of growth rates on load ratio than using K_{max}, suggesting that crack closure greatly influences fatigue-crack propagation in these composites.

IV. DISCUSSION

A. *Fracture Toughness Behavior*

The present study clearly demonstrates that the toughening of $MoSi_2$ can be most effectively achieved under monotonic loading through the incorporation of a high-aspect ratio ductile phase; indeed, in the current work, the use of randomly oriented Nb-wire mesh reinforcements (with $h/r \sim 7$ to 13) led to more than a threefold increase in the toughness of $MoSi_2$ at ambient temperature, compared to a mere ~20 pct increase with spherical Nb reinforcements. Moreover, due primarily to extensive crack deflection along the weak Nb-phase reaction-layer interfaces,* consequent

*The extensive debonding along reaction-layer interfaces in $Nb/MoSi_2$ intermetallic systems can be associated with the mismatch in thermal and elastic properties across the $Nb/Mo_5Si_3/MoSi_2$ interfaces. For discussion, see Ref. 14.

crack bridging by the ductile phase, and possible crack blunting within this phase, the fracture behavior of the $MoSi_2$ composite is associated with stable crack growth along the R curve. With this toughening approach, a steady-state toughness of 13 MPa$\sqrt{m}$ has been achieved, which is believed to be one of the highest toughness reported for a $MoSi_2$-based material to date.* Subsequently, we examine this behavior in light of some simple toughening models for crack bridging and crack deflection.

*Fracture toughness values as high as 15 MPa$\sqrt{m}$ have been claimed for 20 vol pct Nb-reinforced $MoSi_2$ laminates.[25] However, such data were derived from peak load measurements on chevron-notched samples which did not contain sharp (*i.e.*, fatigue) precracks.

1. *Ductile-phase toughening models*

The extent of toughening induced by ductile-particle bridging can be estimated using a simple approach that accounts for the increase in energy associated with particle deformation and failure in the crack wake. When the length of the bridging zone is small compared to the specimen and crack length dimensions, *i.e.*, small-scale bridging conditions exist, the toughness increases with crack extension up to a maximum steady-state level, K_{ssb}, associated with the development of a steady-state bridging zone length, l_{ssb}. At this small-scale bridging limit, K_{ssb}, is given as[45,46]

$$K_{ssb} = \sqrt{K_t^2 + E' f r \sigma_0 \chi} \qquad [4]$$

where K_t is the crack-initiation toughness of the composite (often taken as the matrix toughness, or the stress intensity for crack renucleation); E' is the plane-strain elastic modulus of the composite ($= E/(1 - \nu^2)$, ν being the Poisson's ratio); and σ_0, f, χ, and r refer to the yield strength, volume fraction, work of rupture, and the characteristic dimension of the reinforcement, respectively. The nondimensional work of rupture, χ, is taken to be the area under the normalized-particle stress [$\sigma(u)$]-displacement[u] function as[21]

$$\chi = \int_0^{u^*} \frac{\sigma(u)du}{\sigma_0 r} \qquad [5]$$

where u^* is the critical crack-opening displacement for failure of the ductile phase. Measurements of χ, made on model Nb/$MoSi_2$ single-fiber composites and single-ply laminates,[24] yield values between ~0.25 and 1.5 depending upon the extent of debonding. In the present calculations, for a debond length of ~0 to 5r, a value of $\chi \sim 0.25$ was assumed. The volume fraction and characteristic radius of the ductile phase were corrected for the presence of the reaction layer; values of $f \sim 0.12$ and $r \sim 60$ μm were used. Taking a value of the flow stress (average of the yield and ultimate tensile) for Nb of $\sigma_0 \sim 170$ MPa,[18] the composite elastic modulus as $E \sim 372$ GPa (using the rule of mixtures where $E_{MoSi_2} \sim 440$ GPa and $E_{Nb} \sim 100$ GPa), and a crack-initiation toughness of $K_t \sim 4.8$ MPa$\sqrt{m}$, the resulting composite toughness from Eq.[4] is predicted to be 12 MPa$\sqrt{m}$, which is comparable to the experimentally measured value of 13 MPa$\sqrt{m}$.

Despite the apparent good agreement, several other factors should be recognized. These include (1) the possible elevation in the yield strength of the Nb phase due to solid-solution strengthening from the diffusion of Si from the matrix;[35,36] (2) variation in the value of χ (χ values were derived from the rupture of the Nb phase in model composites,[24] where extensive plastic deformation precedes fracture, whereas in the present composite, many Nb ligaments failed by a brittle cleavage mechanism); and (3) extensive crack deflection along the Nb/$MoSi_2$ interface, which reduces the area fraction of Nb particles participating in crack bridging processes.

2. *Crack bridging and deflection models*

An alternative approach is provided by the small-scale bridging model of Budiansky *et al.*[47] for particulate reinforcements. Here, using the same nomenclature as in Eq. [4], the composite toughness due to bridging, K_{ssb}, can be estimated by assuming that the crack faces are connected by particles which act as rigid plastic springs and provide uniform tractions ($\sigma = f\sigma_0$) within the bridging zone, l_{ssb}, *viz.*

$$K_{ssb} = K_t + 2 f \sigma_0 \sqrt{\frac{2l_{ssb}}{\pi}} \qquad [6]$$

where f and σ_0 are volume fraction and flow stress of the ductile phase. Taking $f \sim 0.12$, $\sigma_0 \sim 170$ MPa, and $l_{ssb} \sim 1.5$ mm for $Nb_m/MoSi_2$ and the composite initiation toughness of $K_t \sim 4.8$ MPa$\sqrt{m}$ gives a predicted steady-state composite toughness, K_{ssb}, of ~6.1 MPa$\sqrt{m}$, *i.e.*, significantly lower than the experimentally measured value.

However, the preceding estimate is based on bridging effects alone and does not include any contributions from strain hardening within the bridge itself or from the tilting and twisting of the crack path as it encounters the reinforcement. Elastic solutions[22,48] for such deflection of the crack path suggest that, for a microstructure consisting of randomly distributed rod-shaped reinforcements, the reduction in the stress intensity at the crack tip due to in-plane tilting of the crack is minimal, while the out-of-plane twisting contribution is greatly enhanced by the high aspect ratio of the reinforcements. This twisting contribution can be evaluated by considering the statistical spacing between reinforcements and incorporating the corresponding probabilities of crack-reinforcement interception. Based on this approach,[22] a toughening ratio due to deflection (including both twist and tilt) can be defined in terms of the ratio of the critical stress intensities necessary for crack propagation along a deflected and undeflected path, $\lambda_d = K_d/K_t$. For the present $Nb_m/MoSi_2$ composite, where the average aspect ratio, h/r, of the Nb wires is ~10 with $f = 0.12$, the analysis of Faber and Evans[22] predicts the toughening ratio due to deflection, λ_d, to be of the order of 1.7.

Since the corresponding toughening ratio due to the bridging $\lambda_{br} = K_{ssb}/K_t \sim 1.26$, using the principle of superposition and recognizing that crack deflection is responsible for inducing bridging-type behavior, the combined toughening increment due to bridging and deflection, $\lambda = \lambda_{br}\lambda_d$ is of the order of 2.14. This yields a predicted toughness of ~10.3 MPa$\sqrt{m}$ for the $Nb_m/MoSi_2$ composite, some 20 pct lower than the experimentally measured value of 13 MPa$\sqrt{m}$. However, it must be remembered that this analysis includes no contribution from strain hardening within the Nb bridge; more precise modeling should consider the stress-displacement functions to account accurately for the bridging tractions.

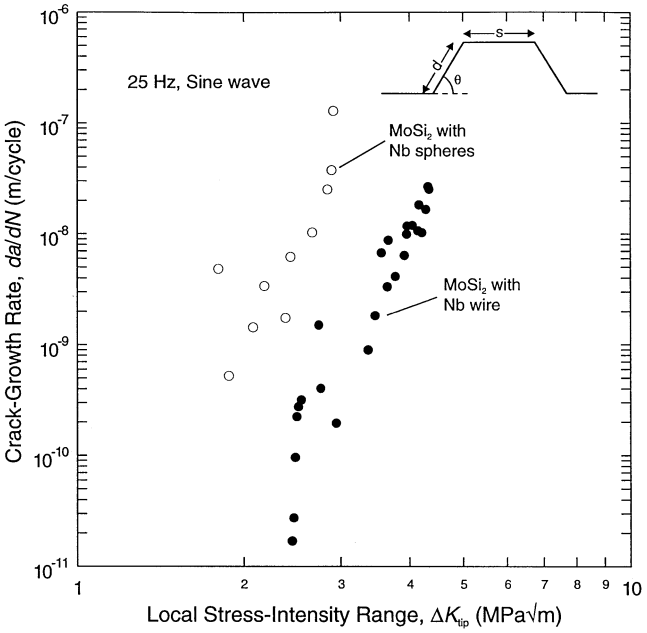

Fig. 13—Variation in cyclic fatigue-crack growth rates, da/dN, for $R = 0.1$, in the $Nb_m/MoSi_2$ and $Nb_p/MoSi_2$ composites as a function of the local stress-intensity range, ΔK_{tip}, to allow for the influence of both crack deflection and crack closure.

B. *Cyclic Fatigue Behavior*

The reinforcement of $MoSi_2$ with high aspect-ratio Nb wires clearly confers far superior resistance to cyclic fatigue-crack growth, in addition to improved fracture resistance, compared to spherical Nb-particulate reinforcements. Moreover, the composite shows far higher fatigue resistance than unreinforced $MoSi_2$;$Nb_m/MoSi_2$ has a fatigue threshold of ~ 7 MPa$\sqrt{m}$ (at $R = 0.1$), whereas unreinforced $MoSi_2$ fails catastrophically at ~ 5 MPa$\sqrt{m}$ with little evidence of subcritical crack growth under cyclic loading. However, similar to many ductile-phase toughened composite systems,[19,39,40] the effect of the reinforcement in improving crack-growth resistance is lower under cyclic loading compared to that under monotonic loads.

Two primary factors appear to influence the cyclic fatigue-crack growth response in the $Nb_m/MoSi_2$ composites. The cycle-dependent degradation in the ductile-phase bridging due to Nb particle failure is principally responsible for the suppression in crack-tip shielding and consequently reduced toughening under cyclic loading; similar effects have been reported in ductile-phase toughened γ-TiAl and Nb_3Al alloys.[19,39,40] However, extensive crack deflection at the Nb/$(Nb,Mo)_5Si_3$ reaction-layer interface (similar to behavior under monotonic loading), interface debonding, and frictional sliding between mating crack-face asperities are all observed fractographically under cyclic loading; furthermore, compliance measurements indicate high levels of crack closure, at least at low load ratios. It is therefore reasoned that the shielding resulting from such mechanisms, namely, crack deflection and roughness-induced crack closure, is primarily responsible for improved fatigue crack-growth properties in the $Nb_m/MoSi_2$ composite.

Shielding from such mechanisms is not uncommon in fatigue and is characteristic of fatigue-crack growth in many metallic materials,[49] especially at low load ratios and close to the fatigue threshold. In the $Nb_m/MoSi_2$ material, deflection and tortuosity of the crack path along the reaction-layer interface lead to a lower near-tip ''driving force'' for crack extension; this, in turn, gives rise to a rougher fracture surface leading to increased crack wedging between surface asperities. Indeed, this notion is supported by the nonlinear crack-path profiles (Figure 7), the rough fracture surface topography (Figure 8), and the high measured crack closure levels at low load ratios which are progressively diminished with increasing R (Figure 9).* Marked crack deflections are clearly apparent in Figure 7 (c) as the crack encounters the Nb wires, where tilt angles can be as high as 60 to 90 deg; the resultant mode II shear at the interface then promotes frictional sliding and generation of wear debris. Furthermore, pronounced closure effects at low R are also consistent with the strong load-ratio dependence of growth rates in this composite (Figure 10).

*In general, the effect of crack closure is diminished at high load ratios because of the larger maximum crack-opening displacements associated with high R cycling.

It is therefore feasible to rationalize such behavior, specifically the improved fatigue resistance of the Nb-mesh reinforced composite compared to that with spherical reinforcements, using simple models for crack deflection[50] and roughness-induced crack closure[51] First-order corrections, to both the local stress-intensity range and the crack-growth rate, for a fatigue crack undergoing periodic (in-plane) deflections can be applied by characterizing the average crack-path deflection in terms of a kink angle θ, the length of the kink d along this direction, and the distance s over which the plane of the growing crack is normal to the far-field tensile axis (insert in Figure 13), *viz.*[50]

$$\Delta K_{tip} = \Delta K_{eff}\left[\hat{d}\cos^2\left(\frac{\theta}{2}\right) + (1 - \hat{d})\right] \qquad [7]$$

$$\left(\frac{da}{dN}\right) = \left(\frac{da}{dN}\right)_L \{\hat{d}\cos\theta + (1 - \hat{d})\} \qquad [8]$$

where ΔK_{eff} is the effective stress-intensity range following the closure correction and ΔK_{tip} is the near-tip driving force after further accounting for crack deflection; da/dN_L and da/dN are the growth rate of the undeflected straight crack and the apparent growth rate for a periodically deflected crack, respectively, and $\hat{d} = d/(d + s)$.

To rationalize the effects of both crack deflection and closure, Eqs.[7] and [8] are applied to the crack-growth rate data for the $Nb_m/MoSi_2$ composite in Figure 12 assuming an average kink angle of ~ 75 deg with $d \sim 2/3$ (*e.g.*, Figure 7); results are plotted in Figure 13 and compared to the previous data for $Nb_p/MoSi_2$.[14] Although there is clearly considerable scatter in the growth-rate data and the load-ratio dependence is unaffected by the deflection corrections, differences between the particulate and wire reinforcement data are greatly reduced (cf., Figure 6) after taking into consideration the effects of both crack deflection and closure. The normalization must be viewed in light of experimental uncertainties associated with K_{cl} measurement, especially in the presence of bridging (if any) and the rather simple nature of the models. However, deflection and crack closure phenomena do appear to provide a rational explanation for the superior fatigue resistance of the Nb-wire

reinforced composite compared to $MoSi_2$ reinforced with spherical Nb particulate and the marked dependency of the crack-growth rates on the load ratio.

V. CONCLUSIONS

Based on a comparison of the fracture toughness/R curve and cyclic fatigue-crack growth properties of the intermetallic compound molybdenum disilicide, reinforced with ductile phases in the form of either a high-aspect ratio Nb-wire mesh ($Nb_m/MoSi_2$) or spherical Nb particles ($Nb_p/MoSi_2$), the following conclusions can be made.

1. The addition of the Nb-wire mesh reinforcement provided significant toughening in $MoSi_2$ at ambient temperatures. Compared to unreinforced $MoSi_2$ or $MoSi_2$ reinforced with spherical Nb particles, where unstable fracture occurred at K_c values of ~5 MPa$\sqrt{m}$ or less, the Nb mesh/$MoSi_2$ composite exhibited rising R-curve behavior with a steady-state fracture toughness of ~13 MPa$\sqrt{m}$.
2. Such improved fracture resistance of the Nb_m-reinforced composite was associated with extensive crack deflection along the weak $(Nb,Mo)_5Si_3$ reaction-layer interfaces and the renucleation of cracks ahead of the Nb wires; both phenomena resulted in extensive crack bridging by the unbroken ductile phase. This explanation was found to be quantitatively consistent with models for crack deflection and crack bridging.
3. The cyclic fatigue-crack growth properties of the $Nb_m/MoSi_2$ composite were also found to be far superior to the $Nb_p/MoSi_2$ material and pure $MoSi_2$, although the degree of improvement was lower than for monotonic loading. Compared to a fatigue threshold, $\Delta K_{TH} \sim 2$ MPa$\sqrt{m}$ (at $R = 0.1$) in the particulate composite, no fatigue cracking could be detected below a ΔK_{TH} of 7 MPa$\sqrt{m}$ in the mesh-reinforced composite. No stable fatigue-crack growth could be detected in monolithic $MoSi_2$.
4. The superior cyclic fatigue-crack growth behavior of the mesh-reinforced composite was also associated with extensive crack deflection along the weak $(Nb,Mo)_5Si_3$ reaction-layer interfaces. Although crack bridging by the ductile phase was largely suppressed under cyclic loading due to premature failure of the Nb wires, the highly deflected crack paths resulted in rough fracture surfaces and accordingly in high levels of crack closure at low load ratios.
5. Similar to many metals and ceramics, fatigue-crack growth rates in the $Nb_m/MoSi_2$ composite were observed to increase, and ΔK_{TH} thresholds to decrease, with increasing load ratio (for $0.1 \le R \le 0.7$). Growth rates were found to show a strong dependence on both K_{max} and ΔK, and unlike ceramics, the *da/dN* data could not be solely normalized in terms of K_{max}.
6. The improved cyclic fatigue-crack growth behavior was found to be quantitatively consistent with simple models for crack deflection and crack closure. Indeed, first-order deflection and closure corrections to both ΔK and *da*/*dN* were seen to provide a feasible explanation for the marked dependency of growth rates on the load ratio and, more importantly, for the far superior fatigue resistance of Nb-wire mesh reinforced composite compared to $MoSi_2$ containing spherical Nb particulate.

ACKNOWLEDGMENTS

This work was supported by the United States Air Force Office of Scientific Research under University Research Initiative Grant No. F49620-93-1-0289 to the University of Michigan, Ann Arbor, MI. Special thanks are due to Dr. S.M. Pickard and Professor Amit K. Ghosh, the University of Michigan, for processing the $Nb_m/MoSi_2$ material, and to the National Science Foundation for an NSF Graduate Fellowship in support of ALM.

REFERENCES

1. J.J. Petrovic and A.K. Vasudévan: in *Intermetallic Matrix Composites II*, Materials Research Society Symposia Proceedings, D.B. Miracle, D.L. Anton, and J.A. Graves, eds., Materials Research Society, Pittsburgh, PA, 1992, vol. 273, pp. 229-39.
2. E. Fitzer, O. Rubisch, J. Schlichting, and I. Sewdas: *Special Ceram.*, 1973, vol. 6.
3. J. Schlichting: *High Temp.-High Pressure*, 1978, vol. 10, pp 241-69.
4. J.J. Petrovic: *MRS Bull.* 1993, vol. 18 (7), pp. 35-40.
5. R.M. Aikin, Jr.: *Scripta Metall. Mater.*, 1992, vol. 26, pp. 1025-30.
6. F.D. Gac and J.J. Petrovic: *J. Am. Ceram. Soc.*, 1985, vol. 68, pp. C200-C201.
7. D.H. Carter and G.F. Hurley: *J. Am. Ceram. Soc.*, 1987, vol. 70, pp. C79-C81.
8. J.M. Yang and S.M. Jeng: 1991 *J. Mater. Res.*, vol. 6, pp. 505-13.
9. J.J. Petrovic and R.E. Honnell: *J. Mater. Sci.*, 1990, vol. 25, pp. 4453-56.
10. U. Ramamurty, A.S. Kim, S. Suresh, and J.J. Petrovic: *J. Am. Ceram. Soc.*, 1993, vol. 76, pp. 2461-72.
11. U. Ramamurty, S. Suresh, and J.J. Petrovic: *J. Am. Ceram. Soc.*, 1994, vol. 77, pp. 2681-88.
12. T.C. Lu, A.G. Evans, R.J. Hecht, and R. Mehrabian: *Acta Metall. Mater.*, 1991, vol. 39, pp. 1853-62.
13. D.E. Alman and N.S. Stoloff: *Mater. Res. Soc. Symp. Proc.*, 1992, vol. 273, pp. 247-52.
14. K.T. Venkateswara Rao, W.O. Soboyejo, and R.O. Ritchie: *Metall. Trans. A*, 1992, vol. 23A, pp. 2249-57.
15. V.D. Kristic: *Phil. Mag.*, 1983, vol. 48, pp. 695-708.
16. L.S. Sigl, P.A. Mataga, B.J. Dalgleish, R.M. McMeeking, and A.G. Evans: *Acta Metall.*, 1988, vol. 36 (4), pp. 945-53.
17. L.S. Sigl and H.E. Exner: *Metall. Trans. A*, 1987, vol. 18A, pp. 1299-1308.
18. H.C. Cao, B.J. Dalgleish, H.E. Deve, C.K. Elliott, A.G. Evans, R. Mehrabian, and G.R. Odette: *Acta Metall.*, 1989, vol. 37, pp. 2969-77.
19. K.T. Venkateswara Rao, G.R. Odette, and R.O. Ritchie: *Acta Metall. Mater.*, 1992, vol. 40 (2), pp. 353-61.
20. M.G. Mendiratta, J.J. Lewandowski, and D.M. Dimiduk: *Metall. Trans. A*, 1991, vol. 22A, pp. 1573-83.
21. M.F. Ashby, F.J. Blunt, and M. Bannister: *Acta Metall.*, 1989, vol. 37, pp. 1847-57.
22. K.T. Faber and A.G. Evans: *Acta Metall.*, 1983, vol. 31, pp. 565-76.
23. S.M. Pickard and A.K. Ghosh: in *High-Temperature Ordered Intermetallic Alloys VI*, Materials Research Society Symposia Proceedings, J. Horton, I. Baker, S. Hanada, R.D. Noebe, and D.S. Schwartz, eds., Materials Research Society, Pittsburgh, PA, 1995, vol. 364, pp. 905-10.
24. S.M. Pickard and A.K. Ghosh: *Metall. Mater. Trans. A*, 1996, vol. 27A, pp. 909-21.
25. L. Xiao, Y.S. Kim, R. Abbaschian, and R.J. Hecht: *Mater. Sci. Eng. A*, 1991, vol. A144, pp. 277-85.
26. A.G. Metcalfe and M.J. Klein: *Composite Materials—Interfaces in Metal Matrix Composites*, Academic Press, New York, NY, 1974, vol. 1.
27. H. Chang, H. Kung, and R. Gibala: in *Intermetallic Matrix Composites II*, Materials Research Society Symposia Proceedings,

D.B. Miracle, D.L. Anton, and J.A. Graves, eds., Materials Research Society, Pittsburgh, PA, 1992, vol. 273, pp. 253-58.
28. C.J. Gilbert, J.M. McNaney, R.H. Dauskardt, and R.O. Ritchie: *ASTM J. Test. Eval.*, 1994, vol. 22 (2), pp. 117-20.
29. R.O. Ritchie, W. Yu, and R.J. Bucci: *Eng. Fract. Mech.*, 1989, vol. 32, pp. 361-77.
30. *Annual Book of ASTM Standards*, ASTM, Philadelphia, PA, 1993, vol. 3.01.
31. R.H. Dauskardt and R.O. Ritchie: *Closed Loop*, 1989, vol. 17, pp. 7-17.
32. W. Elber: *Eng. Fract. Mech.*, 1970, vol. 2, pp. 37-45.
33. S. Suresh and R.O. Ritchie: in *Fatigue Crack Growth Thresholds Concepts*, D.L. Davidson and S. Suresh, eds., TMS-AIME, Warrendale, PA, 1984, pp. 227-61.
34. R.O. Ritchie and W. Yu: in *Small Fatigue Cracks*, R.O. Ritchie and J. Lankford, eds., TMS-AIME, Warrendale, PA, 1986, pp. 167-89.
35. J. Kajuch, J.D. Rigney, and J.J. Lewandowski: *Mater. Sci. Eng. A*, 1992, vol. A155, pp. 59-65.
36. J. Kajuch, J. Short, and J.J. Lewandowski: *Acta Metall. Mater.*, 1995, vol. 43, pp. 1955-67.
37. P.C. Paris and F. Erdogan: *J. Basic Eng., Trans. ASME*, 1963, Ser. D, vol. 85, pp. 528-34.
38. R.O. Ritchie and R.H. Dauskardt: in *The Encyclopedia of Advanced Materials*, D. Bloor, R.J. Brook, M.C. Flemings, and S. Mahajan, eds., Pergamon, Oxford, United Kingdom, 1994, vol. 2, pp. 791-98.
39. K.T. Venkateswara Rao, G.R. Odette, and R.O. Ritchie: *Acta Metall. Mater.*, 1994, vol. 42, pp. 893-911.
40. L. Murugesh, K.T. Venkateswara Rao, and R.O. Ritchie: *Scripta Metall. Mater.*, 1993, vol. 29, pp. 1107-12.
41. R.H. Dauskardt, M.R. James, J.R. Porter, and R.O. Ritchie: *J. Am. Ceram. Soc.*, 1992, vol. 75, pp. 75-71.
42. R.H. VanStone: *Mater. Sci. Eng.*, 1988, vol. A103, pp. 49-61.
43. C.J. Gilbert, R.H. Dauskardt, and R.O. Ritchie: *J. Am. Ceram. Soc.*, 1995, vol. 78, pp. 2291-300.
44. J.E. Allison: in *Fracture Mechanics: Eighteenth Symposium*, ASTM STP 945, D.T. Read and R.P. Reed, eds., ASTM, Philadelphia, PA, 1988, pp. 913-33.
45. A.G. Evans and R.M. McMeeking: *Acta Metall.*, 1986, vol. 34, p. 2435.
46. G.R. Odette, B.L. Chao, J.W. Sheckherd, and G.E. Lucas: *Acta Metall. Mater.*, 1992, vol. 40, p. 2381.
47. B. Budiansky, J.C. Amazigo, and A.G. Evans: *J. Mech. Phys. Solids*, 1988, vol. 36, pp. 167-87.
48. B.A. Bilby, G.E. Cardew, and I.C. Howard: *Fracture 1977*, Proc. 4th Int. Conf on Fracture, D.M.R. Taplin, ed., Pergamon Press, New York, NY, 1977, vol. 3, pp. 197-212.
49. R.O. Ritchie: *Mater. Sci. Eng.*, 1988, vol. A103, pp. 15-28.
50. S. Suresh: *Metall. Trans. A*, 1985, vol. 16A, pp. 249-60.
51. S. Suresh and R.O. Ritchie: *Metall. Trans. A*, 1982, vol. 13A, pp. 1627-31.